GEOPHYSICAL RESEARCH LETTERS, VOL. 27, NO. 16, PAGES 2545-2548, AUGUST 15, 2000

Atmospheric Manifestation of Tropical Instability Wave Observed by QuikSCAT and Tropical Rain Measuring Mission

W. Timothy Liu, Xiaosu Xie, Paulo S. Polito

Jet Propulsion Laboratory, California Institute of Technology, Pasadena, CA

Shang-Ping Xie

International Pacific Research Center, University of Hawaii, Honolulu

and Hiroshi Hashizume

Graduate School of Environment and Earth Science, Hokkaido University, Sapporo, Japan

Abstract. Observations from two new spaceborne microwave instruments in 1999 clearly reveal the atmospheric manifestation of tropical instability waves north of the Pacific equatorial cold tongue. A unique zonal-temporal bandpass filter enables the isolation of the propagating signals and the determination of their phase differences. The phase differences between the propagation of wind and sea surface temperature (SST) signals observed from space and the vertical wind profiles measured from a research ship are consistent with the hypothesis that the coupling between wind and SST is caused by buoyancy instability and mixing, which reduces the wind shear in the atmospheric boundary layer. The coupling causes higher evaporative cooling over the warm phase and infers a negative thermal feedback.

1. Introduction

Tropical instability waves (TIW) vary in exact location and phase velocity. Such waves were best observed by radiometers on geostationary satellites as meanders of the temperature front between the cold upwelling water of the Pacific equatorial cold tongue and the warm water to the north [e.g., Legeckis, 1977; Yoder et al., 1994]. The waves propagate westward, with period of approximately 30 days, wavelength of 1100 km, and phase speed of 0.5 m/s. The waves are stronger from June to November and during La Nina episodes. Sea surface temperature (SST), however, is often obscured from visible and infrared radiometers by cloud cover. When such sensors are on polar orbiting spacecraft, many days of data are need to form a composite map of TIW.

The ocean circulation associated with TIW has been well studied using in situ measurements [e.g., Hansen and Paul, 1984; Halpern et al., 1988; Qiao and Weisberg, 1995; Flamant et al., 1996; Baturin and Niiler, 1997]. The TIW is believed to be generated by the shear of ocean currents and not by local winds. The atmospheric manifestations of the TIW were observed and inferred in a number of studies [e.g., Hayes et al., 1989; Deser et al., 1993]. The sparsity of historical ship data may have limited their use to seasonal and interannual variations of air-sea coupling. The studies of Halpern et al. [1988] and Hayes et al., [1989] were based only on mooring data at fixed locations.

Xie et al. [1998] identified TIW in the wind variations observed by the radar scatterometer on the European Remote Sensing (ERS-1) satellite. They found that the wind divergence patterns propagate westward with their centers sandwiched between the warm and cold poles of the SST. A scatterometer measures both wind speed and direction near the ocean surface. The ERS-1 scatterometer scans a 479 km swath and covers only 40% of the global ocean daily and the wind vector retrieved has a resolution of 50 km. The weekly averaged winds used by Xie et al. [1998] can barely resolve TIW and is not adequate for reliable determination the relative phase between wind and SST, which is key to infer physical mechanism.

Because the atmosphere and the clouds are transparent to microwave, the coincident measurements of two spaceborne microwave instruments during the La Nina episode in the second half of 1999 provided the unprecedented opportunity to observe the influence of the SST front on atmospheric parameters, under both clear and cloudy conditions. The microwave imager on the joint US/Japan Tropical Rainfall Measuring Mission (TRMM) has provided measurements of SST, surface wind speed (WS), and integrated water vapor (WV) in the atmosphere since November 1997. The low-inclination orbit of TRMM is designed to give an optimal sampling rate for monitoring diurnal variations. A radar scatterometer called SeaWinds was launched in June 1999 on NASA's QuikSCAT mission. It has a continuous swath of 1,800 km, providing wind vector measurements at 25 km resolution over 90% of the global ocean daily.

The satellite data also aided the planning of a research cruise on Japan Fishery Agency's R/V Shoyo Maru to observe the vertical structures of the TIW-induced atmospheric waves for the first time. This paper reports briefly on the analysis of the satellite and in situ data with respect to hypotheses on the atmospheric manifestation of oceanic TIW.

2. Hypotheses

There are two hypotheses on the relation between SST and surface winds over tropical oceans. As illustrated by

Paper number 2000GL011545.
0094-8276/00/2000GL011545$05.00

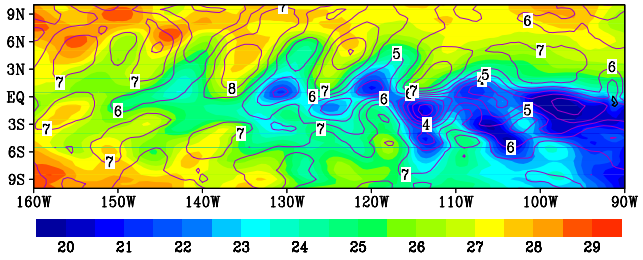

Figure 1. Sea surface temperature (color image, ° C) observed by TMI and surface wind speed (contour, m/s) observed by SeaWinds on 11 September 1999. The temporal means are added back to the anomalies which are bandpass-filtered with a two-dimensional (temporal and longitudinal) filter.

Hayes et al. [1989], they can be differentiated by the phase difference between SST and the two wind components. In the first hypothesis, SST couples with sea level pressure and change the wind [Lindzen and Nigam, 1987]. Lower and higher pressures are found over warmer and cooler water, respectively. As zonal winds (U) move down the pressure or up the temperature gradients, U will always be 90° out of phase with SST and in phase with the zonal gradient of SST. The meridional component (V) is accelerated northward at both the crest (north) and trough (south) of the waves. At the crest, the ocean is cold and V is 180° out of phase with SST. At the trough, the ocean is warm and V is in phase with SST. The strongest wind should be found at the highest pressure or SST gradient. WS is in phase with SST gradient but 90° out of phase with SST.

In the second hypothesis, SST is coupled with wind through the stability (density stratification) change in the atmospheric boundary layer [e.g., Wallace et al., 1989]. Over warm water, air is more buoyant, mixing increases, and wind shear is reduced in the boundary layer; surface winds increase as a consequence. The opposite is true over cold water. WS is in phase with SST. Liu [1990] demonstrated the

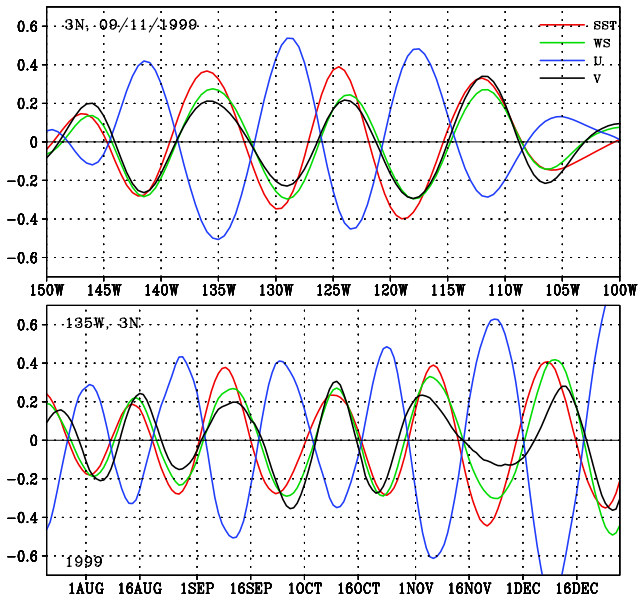

Figure 2. Longitudinal variations at 3°N on 11 September 1999 (a), and time series at 3°N, 135°W (b), of the filtered anomalies of four spacebased parameters.

Table 1. Percentage standard deviation (σ) and phase difference (θ) of the filtered data averaged in the region between 1.5°N and 3.5°N; 105°W and 145°W.

	SST	U	V	WS	WC	WV	LH
σ	56%	24%	40%	49%	50%	23%	39%
&	SST U	SST V	SST WC	SST WS	SST LH	WC WV	
θ	-155°	-11°	-70°	14°	7°	18°	

relative effects of vertical moisture and temperature gradients in destabilizing the atmosphere over the tropical oceans. The prevailing wind aloft is from the southeast. Mixing winds aloft down to the surface over warm water increase the northward (positive) and the eastward (negative) components of surface wind. The results are that U will be 180° out of phase and V will be in phase with SST.

3. Spacebased data

SeaWinds and TRMM Microwave Imager (TMI) data from 21 July to 28 December 1999 were used in this study. The interim data product of SeaWinds were interpolated by a successive correction method [Liu et al., 1998] to uniformly gridded fields of 0.5° latitude by 0.5° longitude and daily resolutions. Wind convergence (WC) was computed from the gridded data. The SST, WV, and WS data from TMI [Wentz, 1997] were acquired as bin averages at 0.25° latitude by 0.25° longitude and daily resolution, separated according to ascending and descending orbits. The ascending and descending data were then averaged together to form daily and 0.5° gridded fields. From TMI SST, WV, and WS, ocean surface latent heat flux (LH) was derived using the methodology developed by Liu [1988]. Liu et al. [1991] indicated that the methodology is less accurate at periods shorter than 10 days, but for the purpose of examining the phase differences between LH and SST, the absolute accuracy of the LH will not affect the results.

The anomaly fields of U, V, WS, and WC from SeaWinds and SST, WV, and LH from TMI, were computed by remov-

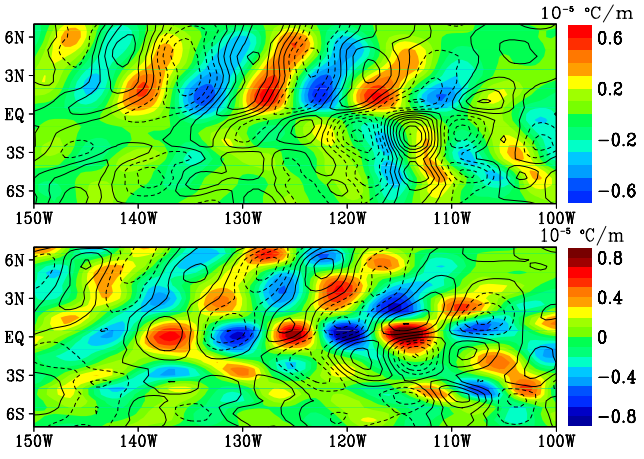

Figure 3. (a) Anomalies of zonal wind component (contours, m/s) superimposed on zonal gradient of SST (color), and (b) meridional wind component superimposed on meridional gradient of SST, for 11 September 1999. The contour interval is 0.5 m/s. The maps are based on filtered SeaWinds and TMI data.

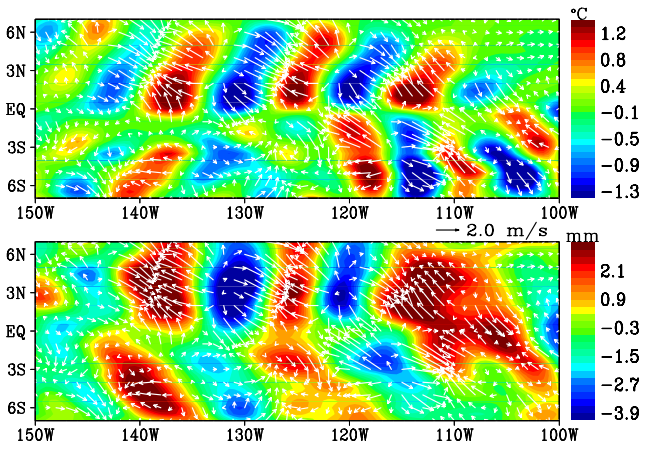

Figure 4. Vector winds anomalies (white arrows) are superimposed on the color images of SST anomalies (a), and water vapor anomalies (b), for 11 September 11 1999, based on filtered data.

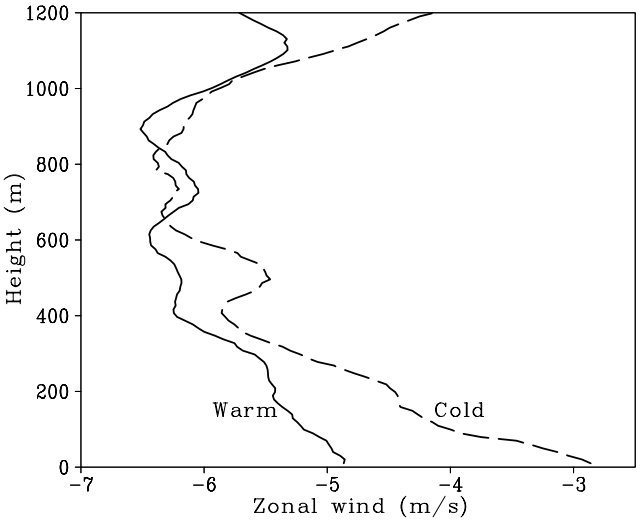

Figure 6. Composite profiles of zonal wind velocity as a function of height over warm (>0.5°C) and cold (<-0.5°C) SST anomalies, measured during a research cruise across TIW.

ing the temporal means. The anomaly fields were band-pass filtered using two-dimensional zonal-temporal finite impulse response (FIR) filters to isolate the TIW. The filters produce practically no phase distortion and a smooth transition between the stop and pass bands. The FIR filters require prior knowledge of the signal (approximate phase speed and period to within a factor of two) as input. Details of the filter are given by Polito et al. [2000]. Table 1 shows that considerable portions of the variances are in the TIW, but the portion of variances in filtered U and WV anomalies are relatively small. The unique filter helped to reveal these weak signals. The filtered SST and WS (with temporal mean added) in Fig. 1 show the close relation between the two parameters in a typical day, with higher WS located over warmer water. Wentz et al [2000] observed similar relations between SST and wind speed in the TMI data. The SST pattern from TMI data was also described by Chelton et al. [2000].

4. Phase differences

Table 1 shows that the SST is in phase with WS and V, but roughly opposite in phase (slightly less than 180°) with U. This is consistent with the second hypothesis described in Section 2, that buoyancy-induced mixing reduces wind shear in the boundary layer. The longitude sections in Fig. 2a and the time series in Fig. 2b essentially reinforce the inference. Fig. 3 shows that the wind components are roughly in quadrature with the SST gradients; the results are not consistent with the first hypothesis on pressure-gradient as the driver of wind anomalies, described in Section 2. The phase differences given in Table 1 are averages over an area where TIW is most prominent. The phase differences are less clear near the equator, north of 6°N, east of 110°W, and west of 160°W, where different mechanisms may become important in governing the wind-SST coupling.

Table 1 also shows that WC is roughly in quadrature with U and SST, as expected. As winds move across isotherms of SST, they accelerate and decelerate, causing convergence and divergence centers at maximum SST gradients, as shown in Fig. 4a. Fig. 4b shows that WC are nearly co-located with positive WV anomalies. Wind convergence feeds moisture up into the atmosphere. The increase in atmosphere water vapor may be caused by both the surface warming and wind advection.

LH depends on WS and the sea-air humidity gradient. Fig. 5 and Table 1 both show that LH is in phase with SST and WS. The strong coupling between SST and WS increases evaporative cooling and may dampen the growth TIW. The day (11 September 1999) and the location (3°N and 135°W) used in Fig. 1-5 are arbitrarily chosen for representative results.

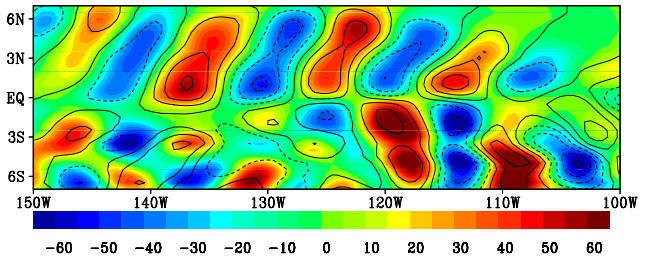

Figure 5. Filtered anomalies of sea surface temperature (contour, ° C) superimposed on latent heat flux (color, W/m^2) for 11 September 1999. The contour interval is 0.5°.

5. Wind profiles

Between 21 and 28 September 1999, the Japanese research vessel, Shoyo Maru, sailed from 140°W to 110°W along 2°N. A Gaussian filter was applied to shipboard measurements to extract TIW-induced SST signals. During the cruise, GPS radiosondes were released to measure the vertical profiles of wind. Five wind soundings were measured with SST anomalies of +0.5°C or greater, and five profiles were found with SST anomalies -0.5°C and lower. They were averaged to form composite profiles over the warm and cold phases of TIW. Fig. 6 shows that the zonal winds are always from the east (negative). Below 600 m, the zonal wind shear is substantially reduced over the warm phase of TIW, resulting in an increase of surface wind speed by more than 2 m/s, which is consistent with the analysis based on

satellite data. The standard deviation of the wind averages at the surface are 0.5 m/s over warm water and 0.8 m/s over cold water; standard deviations in the lowest 300 m are very consistent with these values. Without band-pass filtering, high-level winds are more susceptible to the influences of non-local circulation. The model simulation by Xie et al. [1988] indicated a vertical phase-shift in the profiles of wind anomalies. The one-time cruise section may not have sufficient sampling to reveal two-dimensional changes.

6. Conclusion

Coincident all-weather observations by a spacebased microwave scatterometer and a microwave radiometer during a La Nina episode reveal clearly the atmospheric manifestation of TIW in surface wind vectors and integrated water vapor. The phase differences between wind components and SST determined from the spacebased data and the wind profiles measured on a research cruise are consistent with the hypothesis that buoyancy instability over warm region of TIW reduces vertical wind shear in the atmospheric boundary layer. LH is found to be in phase with SST and WS with possible negative feedback.

The TIW-induced wind fluctuation is about 2 m/s. The ability to detect the spatial structure of this fluctuation on a daily basis as demonstrated in Section 4 attests unprecedented accuracy and time-space resolution of SeaWinds measurements.

This study was confined to the TIW north of the equator in the Pacific, but similar air-sea coupling is obvious south of the equator in Fig. 1, 3, 4 and 5. Atmospheric responses to the TIW in the South Pacific and the Atlantic were investigated by Hashizume et al. [2000].

Acknowledgments. This study was performed at the Jet Propulsion Laboratory, California Institute of Technology, under contract with NASA. It was supported jointly by the QuikSCAT Project, the Tropical Rain Measuring Mission, and the Earth Observing System Interdisciplinary Science Program of NASA. The TMI data were produced by Frank Wentz who generously made his TMI data openly accessible. Processing of cruise data was performed at University of Hawaii. T. Watanabe, M. Shiotani, M. Fujiwara and the crew of the Japan Fisheries Agency's R/V Shoyo Maru successfully conducted the cruise and acquired the in-situ measurements. TMI data are accessible at http://www.ssmi.com and SeaWinds data are available at http://airsea-www.jpl.nasa.gov/seaflux.

References

Baturin, N.G., and P.P. Niiler, Effects of instability waves in he mixed layer of the equatorial Pacific. *J. Geophys. Res.*, *102*, 27,771-27,793, 1997.

Chelton, D. B., F. J. Wentz, C. L. Gentemann, R. A. de Szoeke, M. G. Schlax, Satellite microwave SST observations of transequatorial tropical instability waves. *Geophys. Res. Lett.*, *27*, 1239-1242, 2000.

Deser, C., J.J. Bates, and S. Wahl, The influence of sea surface temperature gradient on stratiform cloudiness along the equatorial front in the Pacific Ocean. *J Climate*, *6*, 1172-1180, 1993.

Flamant, P., S.C. Kennean, R.A. Knox, P.P. Niiler, and R. Bernstein, The three-dimensional structure of an upper ocean vortex in the tropical Pacific ocean. *Nature*, *383*, 610-613, 1996.

Halpern, D., R. Knox, and D.S. Luther, Observations of 20-day period meridional current oscillations in the upper ocean along the Pacific Equator. *J. Phys. Oceanogr.*, *18*, 1514-1534, 1988.

Hansen, D.V., and C.A. Paul, Genesis and effects of long waves in the equatorial Pacific. *J. Geophys. Res.*, *89*, 10,431-10,440, 1984.

Hashizume, H., S.-P. Xie, W. T. Liu, and K. Takeuchi, Local and remote atmospheric response to tropical instability waves: a global view from space. *J. Geophys. Res.*, submitted.

Hayes, S.P., M.J. McPhaden, and J.M. Wallace, The influence of sea surface temperature on surface wind in the eastern equatorial Pacific: weekly to monthly variability. *J. Climate*, *2*, 1500-1506, 1989.

Legeckis, R., Long waves in the eastern equatorial Pacific; a view of a geostationary satellite. *Science*, *197*, 1177-1181, 1997.

Lindzen, R.S., and S. Nigam, On the role of sea-surface temperature gradients in forcing low-level winds and convergence in the tropics. *J. Atmos. Sci.*, *44*, 2440-2458, 1987.

Liu, W.T., Moistures and latent heat flux variabilities in the tropical Pacific derived from satellite data. *J. Geophys. Res.*, *93*, 6749-6760, 1988.

Liu, W.T., Remote Sensing of surface turbulence flux. *Surface Waves and Fluxes*, *Vol. II*,. G.L. Geenaert and W.J. Plant (eds), Kluwer Academic, Chapter 16, 293-309, 1990.

Liu, W.T., W. Tang, and P.P. Niiler, Humidity profiles over oceans. J. Climate, *4*, 1023-1034, 1991.

Liu, W.T., W. Tang, and P.S. Polito, NASA Scatterometer provides global ocean-surface wind fields with more structures than numerical weather prediction. *Geophys. Res. Lett.*, *25*, 761-764, 1998.

Polito, P.S., O.T. Sato, W.T. Liu, Characterization and validation of the heat storage variability from Topex/Poseidon at four oceanographic sites. *J. Geophys. Res.*, in press, 2000.

Qiao, L., and R.H. Weisberg, Tropical instability wave kinematics: observations from the Tropical Instability Wave Experiment. *J. Geophys. Res.*, *100*, 8677-8693, 1995.

Wallace, J.M., T.P. Mitchell, and C. Deser, The influence of sea-surface temperature on surface wind in the eastern equatorial Pacific: seasonal and interannual variability. *J. Climate*, *2*, 1492-1499, 1989.

Wentz, F.J., A well-calibrated ocean algorithm for special sensor microwave / imager, *J. Geophys. Res.*, *102*, 8703-8718, 1997.

Wentz, F.J., C. Gentemann, D. Smith, D. Chelton, Satellite Measurements of Sea Surface Temperature Through Clouds. *Science*, *288*, 847-850, 2000.

Xie, S.P., M. Ishiwatari, H. Hashizume, and K. Takeuchi, Coupled ocean-atmospheric waves on the equatorial front. *Geophys. Res. Lett.*, *25*, 3863-3966, 1988.

Yoder, J.A., S.G. Ackleson, R.T. Barber, P. Flament, and W. M. Balch, A line in the sea. *Nature*, *371*, 689-692, 1994.

W. T. Liu, X. Xie, Paulo S. Polito, Jet Propulsion Laboratory, California Institute of Technology, 4800 Oak Grove Drive, MS 300-323, Pasadena, CA 91109. (e-mail: liu@pacific.jpl.nasa.gov)

Shang-Ping Xie, International Pacific Research Center, University of Hawaii, Honolulu

and Hiroshi Hashizume, Graduate School of Environment and Earth Science, Hokkaido University, Sapporo, Japan

(Received Febuary 29, 2000; revised june 6, 2000;
accepted June 14, 2000.)